Search for Dark Matter Induced Deexcitation of $^{180}Ta^{m}$

Björn Lehnert,[1,*] Harikrishnan Ramani,[2,3,†] Mikael Hult,[4] Guillaume Lutter,[4] Maxim Pospelov,[5,6,7] Surjeet Rajendran,[8] and Kai Zuber[9]

[1]Nuclear Science Division, Lawrence Berkeley National Laboratory, Berkeley, California 94720, USA
[2]Berkeley Center for Theoretical Physics, Department of Physics, University of California, Berkeley, California 94720, USA
[3]Theoretical Physics Group, Lawrence Berkeley National Laboratory, Berkeley, California 94720, USA
[4]European Commission, JRC-Geel, Retieseweg 111, B-2440 Geel, Belgium
[5]School of Physics and Astronomy, University of Minnesota, Minneapolis, Minnesota 55455, USA
[6]William I. Fine Theoretical Physics Institute, School of Physics and Astronomy, University of Minnesota, Minneapolis, Minnesota 55455, USA
[7]Perimeter Institute for Theoretical Physics, Waterloo, Ontario N2J 2W9, Canada
[8]Department of Physics and Astronomy, The Johns Hopkins University, Baltimore, Maryland 21218, USA
[9]Institut für Kern- und Teilchenphysik, Technische Universität Dresden, Zellescher Weg 19, 01069 Dresden Germany

(Received 21 November 2019; revised manuscript received 30 March 2020; accepted 1 April 2020; published 7 May 2020)

Weak-scale dark matter particles, in collisions with nuclei, can mediate transitions between different nuclear energy levels. In particular, owing to sizeable momentum exchange, dark matter particles can enable de-excitation of nuclear isomers that are extremely long lived with respect to regular radioactive decays. In this Letter, we utilize data from a past experiment with $^{180}Ta^{m}$ to search for γ lines that would accompany dark matter induced de-excitation of this isomer. Nonobservation of such transitions above background yields the first direct constraint on the lifetime of $^{180}Ta^{m}$ against dark matter initiated transitions: $T_{1/2} > 1.3 \times 10^{14}$ a at 90% credibility. Using this result, we derive novel constraints on dark matter models with strongly interacting relics and on models with inelastic dark matter particles. Existing constraints are strengthened by this independent new method. The obtained limits are also valid for the standard model γ-decay of $^{180}Ta^{m}$.

DOI: 10.1103/PhysRevLett.124.181802

Introduction.—The existence of massive stable particles with masses commensurate with the electroweak scale is a common feature of many extensions of the standard model (SM) [1]. Such particles can account for the entirety (or a fraction) of dark matter (DM) in the Universe, motivating intense theoretical and experimental efforts to discover them, or else constrain their properties. Indeed, the searches of weakly interacting massive particles (WIMPs) have progressed to probe tiny cross sections of DM particles with nuclei and electrons (see, e.g., [2]), and have become the most prominent endeavor in trying to elucidate its nature.

Nuclear physics, thus far, played a rather limited role in such searches. In most of the large-scale experiments [3–6], the nuclear physics input is often limited to refinement of the nuclear matrix elements (e.g., providing a better treatment of elastic nuclear form factors). Occasionally, ideas with excitation of nuclear levels by WIMPs have been explored as a way of complementing main searches [7–9].

In recent work [10], it was argued that long lived nuclear isomers can be used as a tool for DM searches, offering a unique probe of DM candidates that are, otherwise, undetectable in conventional underground experiments. Interaction with a DM particle may lead to a direct DM-induced de-excitation of an isomer $\mathcal{N}(*)$ to a lower level $\mathcal{N}(0)$

$$\mathcal{N}(*) + \mathrm{DM} \rightarrow \mathcal{N}(0) + \mathrm{DM}, \tag{1}$$

where ΔE, the excess of nuclear energy, is released as the kinetic energy of the final state particles. Crucially, this process need not be kinematically suppressed, as $(R_N k_\gamma)^{2L}$ (here, R_N is the nuclear radius, and k_γ is the wave number of the emitted γ ray, with typical values of 10^{-2} to 10^{-3} for $R_N k_\gamma$) is changed to $(R_N\sqrt{2\Delta E\mu}/\hbar)^{2L}$, where μ is a reduced mass of the DM-nucleus system. The minimum momentum transfer $q_0 = \sqrt{2\Delta E\mu}$ can be as large as $\hbar R_N^{-1}$, so that the main suppression factor can be fully lifted. In this Letter, we implement the first direct search of the process in Eq. (1), taking the isomeric state to be the famous $^{180}Ta^{m}$ nucleus.

The conventional decay of $^{180}Ta^{m}$ was investigated numerous times in the past but has never been observed. The E_7 transition required for the decay of the 9^- isomeric state makes it especially long lived and remarkably stable on cosmological timescales. Additional interest to this nucleus stems from its relatively large abundance ($\simeq 10^{-4}$ of natural tantalum), which is difficult to reconcile with nucleosynthesis models, where odd-odd nuclei such as

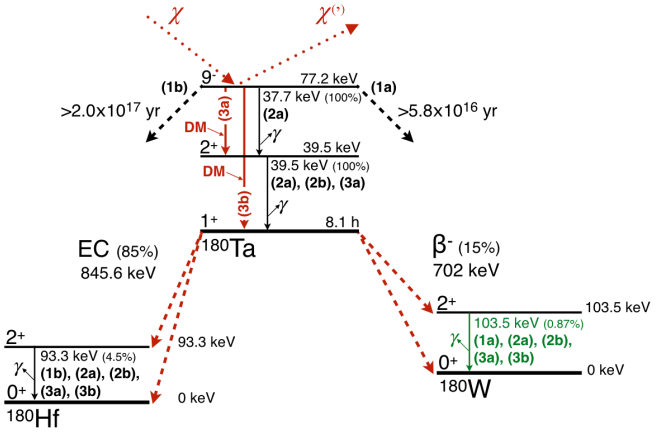

FIG. 1. Decay scheme of ^{180}Ta^{m} with data from [14] illustrating the different decay modes: (1a),(2a) β^- and EC, (2a),(2b) γ decay and internal conversion, (3a),(3b) DM induced decay to 2^+ and 1^+ state. The dark matter interaction with ^{180}Ta^{m} and the investigated decay modes are highlighted in red. For each of the possible γ rays from the ^{180}Ta^{m} decay, their contributing decay modes are shown. The signature γ ray used in this analysis is highlighted in green.

^{180}Ta^{m} are difficult to preserve. Figure 1 shows the possible decay modes of ^{180}Ta^{m} which are listed below: The β^- decay (1a) and electron capture (EC) (1b) are third forbidden nonunique transitions which were recently investigated in [11]. The experimental signatures are the de-excitation γ cascades from the 6^+ excited states of ^{180}W and ^{180}Hf, respectively (not shown). Current half-life limits are at 5.8×10^{16} a for (1a) and 2.0×10^{17} a for (1b) [90% credibility interval (C.I.)] [11], whereas theoretical calculations predict 5.4×10^{23} a for (1a) and 1.4×10^{20} a for (1b) [12,13]. The γ decay (2a) and internal conversion (2b) to the ^{180}Ta ground state is followed by the 8.1 h delayed β^- decay or EC into the ground and first excited states of ^{180}W and ^{180}Hf. The experimental signatures are the 103.5 and 93.3 keV de-excitation γ rays for (2b) and the additional 37.7 and 39.5 keV γ rays for (2a). Theoretical half-life estimates are 1.4×10^{31} a for (2a) and 8×10^{18} a for (2b). The internal conversion mode is predicted to be the dominant decay channel in [12,13].

The DM induced ^{180}Ta^{m} de-excitations $9^- - 2^+$ (3a) and $9^- - 1^+$ (3b) are the focus of this work. The experimental signature for (3b) is identical to (2b), whereas (3a) has the additional 39.5 keV γ ray from the ^{180}Ta 2^+ de-excitation.

Currently, the half-life sensitivity for processes (2) and (3) is well below the theoretical prediction of (2b) at 8×10^{18} a, so then, a nonobservation provides constraints for all decay modes. Should a positive signal eventually be seen, investigation of overburden-dependence will have a discriminating power between natural and DM-induced decays in some models.

Given that only $\sim 10^{-4}$ of natural tantalum can be used for the search, it is clear that the search of reaction in Eq. (1) cannot compete with massive Xe and Ar based experiments for constraining tiny elastic cross sections. Instead, the ^{180}Ta^{m} half-life limit will provide a means for probing DM models that cannot be probed with conventional methods [2]. First, if DM interacts strongly with the SM, it will undergo multiple successive collisions in the atmosphere and overburden, such that its kinetic energy is reduced far below the threshold for any underground DM detector. But even with vanishingly small incoming velocity, the DM-induced de-excitation of ^{180}Ta^{m} will go unimpeded. Rocket and balloon experiments [15,16] with reduced exposures compared to terrestrial direct detection (DD) experiments have been conducted above the atmosphere in order to access DM which has passed through negligible overburden [17,18]. The results we derive in this Letter using tantalum allow us to improve on these bounds and strengthen existing constraints with an entirely different method. Significant progress is achieved in models where strongly interacting massive particles constitute a subdominant component of DM, which is expected in models with thermal DM freeze-out (see, e.g., [19]).

Another class of WIMP models that could escape conventional searches but be discovered or constrained with nuclear isomers are the so-called inelastic DM. In these models, DM is the lighter of two components with a small mass difference, and has dominantly off-diagonal couplings, i.e., inelastic interactions with the SM.

Therefore, the dominant scattering mechanism requires additional energy for DM excitation, and would not proceed if the mass splitting of the two DM states exceeds available kinetic energy. An addition of nuclear excitation energy ΔE provided by the isomer in this case, allows accessing larger mass splitting in the DM sector. Higgsinos arising from supersymmetric theories are an example of a well motivated inelastic DM candidate that would invoke the WIMP miracle to explain the DM relic abundance that is not yet ruled out by DM experiments [20].

Experiment.—In this work, we reanalyzed data collected in [11] to look for the signal corresponding to scattering with DM. The search in [11] focused on excited state transitions from the EC and β^- decays of ^{180}Ta^{m} which includes higher energy γ rays up to 332.3 keV. This search focuses on the 93.3 and 103.5 keV γ rays as a signature of the ^{180}Ta ground state decay. However, the 93.3 keV γ line from the EC branch is overlapped with two background γ lines from ^{234}Th at 92.38 ± 0.01 keV (2.18%) and 92.80 ± 0.02 keV (2.15%), with emission probabilities quoted in parenthesis as well as the Th K-α1 x ray at 93.31 keV. Thus, only the 103.5 keV γ line from the β^- branch is used in the analysis as illustrated in red in Fig. 1. A γ line at 103.35 keV, also from ^{234}Th, has 3 orders of magnitude lower emission probability of 3.2×10^{-5} and is negligible. A search of nuclear data revealed no reasonable lines which could interfere with this measurement. The measurements in [11] were not optimized for such low energy but, nevertheless, can be used to set limits. Future

TABLE I. Overview of the datasets used in the analysis. Columns from left to right denote measurement name, the used HPGe setup, the measurement time, the resolution in FWHM at 103.5 keV, and the detection efficiency for the 103.5 keV γ ray.

Dataset	Setup	Time (d)	FWHM (keV)	ϵ_{det} (%)
M1	singe det.	170	0.62	0.144
M2	2-det sandwich	68	0.70	0.239
M3_Ge6	1-det in sandwich	176	0.70	0.056
M3_Ge7	1-det in sandwich	176	0.58	0.174

experimental improvements are pointed out at the relevant points below and in the Conclusion section.

The target sample consists of six tantalum discs of natural isotopic abundance. The discs have a diameter of 100 mm and a thickness of 2 mm each, summing up to a total mass of 1500.33 g containing 180 mg $^{180}\mathrm{Ta}^{\mathrm{m}}$. In total, three measurements are combined: M1 from [21], M2 from [22], and M3 from [11]. Their parameters are condensed in Table I for the γ line of interest and the recorded spectra are shown in Fig. 2. All measurements were taken at the HADES underground laboratory with 225 m overburden. Measurement M1 was performed on a single HPGe detector, whereas measurements M2 and M3 were performed in a two-detector sandwich setup. In M2, the data of both detectors were combined into one dataset, whereas in M3, they were split into two detectors in order to maximize the advantages of both detector types. Ge6 has a 1.0 mm thick copper window and a 0.7 mm thick dead layer at the top of the Ge crystal, whereas Ge7 has a 1.5 mm thick aluminium window and a 0.3 μm dead layer at the top. The latter is more suitable for the detection of low energy γ rays as can be seen in their detection efficiency of the 103.5 keV γ ray in Table I.

The full energy detection efficiencies were determined with a Monte Carlo code based on EGSNRC [23]. The uncertainty is estimated as 10%.

The analysis is a peak search fitting the Gaussian signal shape on top of an empirical linear background using the Bayesian Analysis Toolkit [24] as described in [11]. The combined fit to all four datasets includes the inverse half-life as the single parameter of interest and is also shown in Fig. 2. Each individual dataset has two parameters to model the linear background, one parameter for the efficiency, one parameter for the resolution and one parameter for the signal peak position. The fit in the energy interval [87,110] keV includes one background γ line from ^{228}Ac at 99.51 keV and two from ^{234}Th at 93.28 and 92.80 keV. The strength of the background γ lines varies between the datasets due to the different detector geometries and setups.

Parameters with known values such as peak positions, the resolution and the detection efficiency have Gaussian priors assigned with the width set to their known uncertainty. This naturally includes systematic uncertainties in the fit. The total efficiency is composed of the emission probability of the 103.5 keV γ ray for the ^{180}Ta ground state decay of $0.87 \pm 0.24\%$ as well as the detection efficiency quoted in Table I with 10% uncertainty. The emission probability dominates to a total uncertainty of 30% for the efficiency parameter. Based on the input parameters, the fit finds zero inverse half-life as the best fit value, and hence, no signal is observed. The limit setting is based on the marginalized posterior distribution of the inverse half-life of which the 0.9 quantile is used as the 90% C.I. at

$$T_{1/2} > 1.3 \times 10^{14}\ \mathrm{a}\,(90\%\,\mathrm{C.I.}). \tag{2}$$

Compared to the partial half-life limits for the β and EC decay modes of $^{180}\mathrm{Ta}^{\mathrm{m}}$ obtained in [11], this half-life limit on the $^{180}\mathrm{Ta}^{\mathrm{m}}$ γ decay is more than 2 orders of magnitude weaker due to the lower emission probability and detection efficiency of the signal γ ray.

Results for dark matter.—We interpret the partial half-life limits obtained above as limits on DM scattering. The relevant process is DM scattering $^{180}\mathrm{Ta}^{\mathrm{m}}$ ($j = 9^-$, $E = 77.2$ keV) to either the lower excited state ($j = 2^+$, $E = 39.5$ keV), i.e., decay mode (3a), or ground state ($j = 1^+$, $E = 0$ keV), i.e., decay mode (3b).

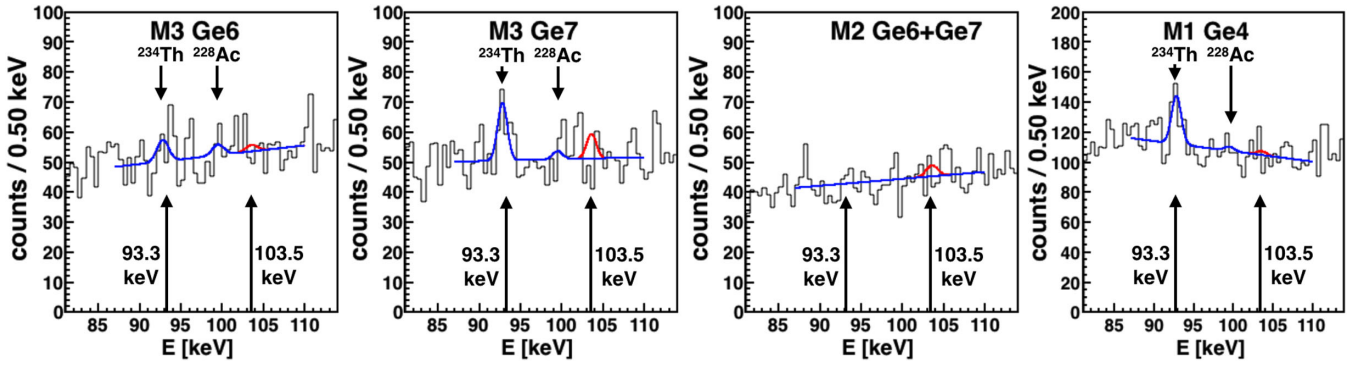

FIG. 2. Region of interest in each dataset for the 103.5 keV peak search in the β^- channel. The best fit is shown in blue, and the best fit with the signal peak set to the 90% C.I. half-life limit is shown in red. The arrows indicated the 93.3 keV peak of the EC channel (not used in fit) as well as the named background γ lines.

Given $T_{1/2}$, a limit can be set on cross-section for DM χ with mass M_χ, to scatter off $^{180}\mathrm{Ta}^{\mathrm{m}}$, $\sigma_{\chi\mathrm{Ta}}$ through

$$\langle \sigma_{\chi\mathrm{Ta}} v_\chi \rangle \leq \frac{M_\chi \log(2)}{T_{\frac{1}{2}} \rho_{\mathrm{lab}}} \tag{3}$$

Here, ρ_{lab} is the local DM density in the lab. Limits on $\sigma_{\chi\mathrm{Ta}}$, thus obtained, can then be used to set limits on model dependent per nucleon cross sections as described next.

DM that interacts strongly with nuclei: DM that interacts strongly with nuclei is poorly constrained due to its slow down in the atmosphere. The slow down can lead to thermalization with the atmosphere or rock overburden, and the presence of the gravitational potential eventually leads to a terminal velocity v_{term} towards the center of the earth. The local downward velocity determines the local DM density through flux conservation, $\rho_{\mathrm{lab}} = (v_{\mathrm{vir}}/v_{\mathrm{term}})\rho_{\mathrm{SS}}$, where ρ_{lab} is the DM density at a location of an underground lab, ρ_{SS} is the solar system (SS) DM density, and v_{vir} is the local virial velocity of DM. The density enhancement $\eta = \rho_{\mathrm{lab}}/\rho_{\mathrm{SS}}$ was evaluated in [10] as a function of σ_n and M_χ for the HADES lab with 225 m overburden. η can reach as large as 10^8 for $M_\chi \sim 100$ GeV and $\sigma_n > 10^{-30}$ cm^2.

For DM lighter than the abundant nuclei on Earth, there is an additional trapped thermalized population which was estimated in [25]. We use this in addition to the density estimated in [10] for limit setting purposes. We provide η as a function of σ_n and relevant M_χ in the Supplemental Material [26].

We model the cross-section as a generic strong-scale interaction, i.e., $\sim 1/\Lambda^2_{\mathrm{QCD}}$ through the exchange of meson-like hadron resonances, and its reference per nucleon cross-section is taken to be σ_n. Following [10], the total cross-section for χ to scatter off $^{180}\mathrm{Ta}^{\mathrm{m}}$ can be estimated by the following ansatz:

$$\langle \sigma_{\chi\mathrm{Ta}} v_\chi \rangle = \mathrm{Min}\left(\sigma_n \frac{\mu_{\mathrm{Ta},\chi}}{q_0}, 4\pi R^2_{\mathrm{Ta}}\right) \mathcal{S}_f(\boldsymbol{q_0}). \tag{4}$$

Throughout this Letter, we use natural units, $\hbar = c = 1$. Here, $\mu_{\mathrm{Ta},\chi}$ is the tantalum-DM reduced mass, $q_0 = \sqrt{\Delta E \times \mu_{\mathrm{Ta},\chi}}$ is the momentum exchange, and R_{Ta} is the radius of tantalum nuclei. The quantity $\mathcal{S}_f(\boldsymbol{q_0})$ is the square of the nuclear form factor that captures the inelastic matrix element for the down scatter of the isomeric state to one of the lower states. Following [10], it is estimated from the Weisskopf estimates and includes the hindrance factor ϵ_H prescribed in [12],

$$\mathcal{S}_f(\boldsymbol{q_0}) = \sum_L \kappa_L j_L^2(qR)\epsilon_H. \tag{5}$$

Here, j_L are the spherical Bessel functions. The sum runs over odd L, $7 \leq L \leq 11$ for (3a) and $L = 9$ for (3b) scattering processes (refer to Fig. 1). The kludge factor κ_L is present to account for deviations from the ansatz that is not captured by the hindrance factors and can be determined by a scattering experiment or observation of the SM decay.

Since it is an exothermic reaction, the counting rate depends on the local DM density and not the flux. We can use Eq. (4) along with η calculated in [10], the relation in Eq. (3) and the limit in Eq. (2) to set limits on σ_n. This limit will depend on f_{DM}, the fraction of Solar System DM in χ particles. Limit contours are plotted in the σ_n vs M_χ plane in Fig. 3 (left) for $f_{\mathrm{DM}} = 10^{-4}$. We also show limits from existing experiments which are adapted from [18]. Stringent new limits are set for $M_\chi > 50$ GeV in the

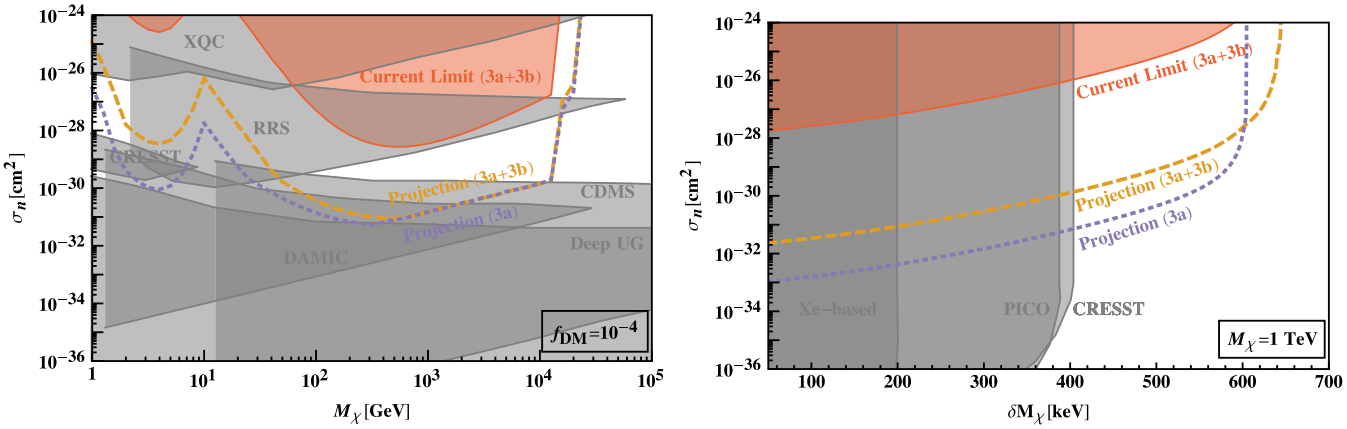

FIG. 3. Left: 90% credibility limits on the per-nucleon cross section for strongly interacting DM. Existing experimental limits are shown in gray (adapted from [18]) and the limit set in this work is shown in red. Future projections for $^{180}\mathrm{Ta}^{\mathrm{m}}$ half-life limits are shown in dashed orange for $T_{1/2} > 1 \times 10^{18}$ a in the (3a) + (3b) mode and in dashed purple for $T_{1/2} > 4 \times 10^{19}$ a in the (3a) only mode. Right: Limits and projections with the same color coding for inelastic DM with mass splitting δM_χ. Existing experimental limits are adapted from [20].

strongly interacting regime. There is a drastic reduction in parameter space ruled out by existing DD experiments for such small dark matter fractions. However, $^{180}\mathrm{Ta}^{\mathrm{m}}$ has a much slower dropoff in sensitivity owing to its unique ability to look for slowed down DM that has a large local number density. Limits for different f_{DM} are discussed in the Supplemental Material [26].

Inelastic dark matter: DM χ could have dominantly nondiagonal couplings with the SM, i.e., scattering relevant to DD is determined by the operator $\mathcal{L} \supset (G_F^{\chi})^2 \bar{\chi}\chi' \bar{N}N$, where N is the target nucleus, χ' is nondegenerate with χ and $\delta M_\chi = M_{\chi'} - M_\chi$. As a result, this energy difference δM_χ has to be supplied by the initial kinetic energy in the center of mass frame in conventional DD experiments. Limits from these are summarized in [20] and plotted in Fig. 3 (right), in gray for $M_\chi = 1$ TeV. The maximum velocity of the truncated DM velocity distribution, as well as the energy thresholds required for detection, ultimately set the limit on the largest splitting that can be probed, $\delta M_\chi \lesssim 400$ keV in CRESST [30] and PICO [31].

The extra energy available for scattering with $^{180}\mathrm{Ta}^{\mathrm{m}}$, can uniquely set limits on models with higher energy splittings. The kinematics for this process, as well as the estimation of the relevant rates, were described in detail in [10]. The largest splitting that can be accessed with an isomeric transition with energy ΔE_N is given by, $\delta M_\chi \lesssim \frac{1}{2}\mu_{\chi m_N}(v_{\mathrm{E}} + v_{\mathrm{esc}})^2 + \Delta E_N$. Here, $v_{\mathrm{E}} = 240$ km/s is the Earth velocity in the Milky Way frame and $v_{\mathrm{esc}} = 600$ km/s is the escape velocity, the cutoff of the Maxwell Boltzmann velocity distribution of DM. Unlike in the case of elastic collisions, the overburden does not have stopping power below the center of mass kinetic energy threshold.

As in the case of strongly interacting DM, $\sigma_{\chi\mathrm{Ta}}$ can be expressed in terms of the per nucleon cross section σ_n and relevant kinematic integrals [10]. We do not repeat this discussion here for brevity. Limits on inelastic DM with mass $M_\chi = 1$ TeV, as interpreted from the limits on the nonobservation of the isomeric transition are displayed in Fig. 3 (right) as the shaded red region. This can be compared with existing limits. The large improvement in threshold arises due to the extra energy available in the isomer as well as not requiring a specific range in recoil energy. However, it is important to note that inelastic DM models with such large cross sections are hard to construct [10].

Conclusion and future experiments.—This analysis demonstrates that current nuclear isomer samples can be used to probe strongly interacting DM. Such particles are too slow to be detectable by conventional experiments since they require an "exothermic" process to make them experimentally observable. Inelastic DM is another class of models that can be probed by such exothermic isomers. New parameter space is excluded and existing constraints are strengthened with a new independent method.

The experimental setup can be further optimized for these searches. The additional γ rays of 37.7 and 39.5 keV from the $^{180}\mathrm{Ta}^{\mathrm{m}}$ γ or DM induced decay would complement the experimental signature and could increase the sensitivity since their emission probability is 100% per decay. However, such low energies require a dedicated γ-spectroscopy setup which must be optimized by (1) selecting a suitable HPGe detector technology, (2) use a HPGe cryostat with a thin entrance window, (3) optimize the source thickness to reduce self-shielding, and (4) use a tantalum sample enriched in $^{180}\mathrm{Ta}$ to further increase exposure without increasing self-absorption. The optimization of this search along these lines is discussed in the Supplemental Material [26]. Assuming an optimized detector setup scaled to 14 detectors, an enrichment to 5.5% $^{180}\mathrm{Ta}^{\mathrm{m}}$ and three years measurement time would result in a sensitivity of 1×10^{18} a for the 103.5 keV search (3a) + (3b) and 4×10^{19} a for the 39.5 keV search (3a), respectively. This sensitivity would also allow us to test the theoretical half-life prediction of the γ-decay mode (2b) from [12]. The projected sensitivities for the strongly interacting DM and inelastic DM are shown in Fig. 3 for the (3a) + (3b) type search in dashed orange and for the (3a) type search in dashed purple. The orange lines have larger thresholds due to the additional energy available for the (3b) scatter but lower sensitivity due to the smaller branching ratio of the 103.5 keV γ ray.

Different detector technologies could be used to advance this search even further. Large area segmented semiconductor detectors with thin dead layers could be used to maximize the detection efficiency and background rejection of the low energy γ rays from a tantalum foil sandwiched in between them [32,33]. Another idea is to operate a tantalum crystal as a cryogenic bolometer below 100 mK [34]. In this target = detector approach, the low energy γ rays do not have to escape the detector and various crystal sizes are possible to fully optimize the signal to background ratio.

The search for DM using these isomers could be improved with additional experimental work that can reduce theoretical uncertainties. Theoretical estimates of hindrance factors from [12] were used in this work to account for the hitherto unmeasured transition matrix element. This is an order of magnitude estimation which could be more accurately determined by observing the decay or through scattering with SM projectiles. Until now, photons [35] and neutrons [36] have been used to scatter with $^{180}\mathrm{Ta}^{\mathrm{m}}$ to produce de-excitations, albeit the interaction has always gone through a compound nucleus or excited state, since both the photon or neutron can be absorbed. Inelastic scattering with electrons which have been used to estimate transition charge densities for large ΔJ transitions [37], could be repeated for $^{180}\mathrm{Ta}^{\mathrm{m}}$. Additionally, the emission probability of the 103.5 keV γ ray has a large uncertainty of 28%. While this uncertainty is correctly taken into account in the prior probability of the Bayesian

analysis, it would help future experiments to determine the emission probability more precisely.

Furthermore, as pointed out in [10], interesting inelastic DM parameter space can be probed using existing samples of $^{178\,m}$Hf and $^{137\,m}$Ba produced as fission waste. These searches require more sophisticated experimental setups, but given the generic nature of the proposed search and the demonstrated feasibility of the approach, we believe that it would be opportune to perform such searches in these isomers.

We would like to thank Alexey Drobizhev and Vivek Singh for discussions on alternative detector technologies. We also thank Aaron C. Vincent and Ningqiang Song for pointing out a bug in our code that affects the inelastic limits in the previous version by a small amount. This has been corrected in the new version. S. R. was supported in part by the NSF under Grant No. PHY-1638509, the Simons Foundation Grant No. 378243, and the Heising-Simons Foundation Grants No. 2015-038 and No. 2018-0765. H. R. is supported in part by the DOE under Contract No. DE-AC02-05CH11231. The work in HADES by Gerd Marissens, Heiko Stroh, and the Euridice staff is gratefully acknowledged. The measurements were enabled though the Joint Research Centre open access initiative to HADES, Projects No. 21–14.

*bjoernlehnert@lbl.gov
†hramani@berkeley.edu

[1] G. Bertone, D. Hooper, and J. Silk, Particle dark matter: Evidence, candidates and constraints, Phys. Rep. **405**, 279 (2005).
[2] M. Schumann, Direct Detection of WIMP Dark Matter: Concepts and Status, J. Phys. G **46**, 103003 (2019).
[3] E. Aprile *et al.*, Dark Matter Search Results from a One Ton-Year Exposure of XENON1T, Phys. Rev. Lett. **121**, 111302 (2018).
[4] D. S. Akerib *et al.*, Results from a Search for Dark Matter in the Complete LUX Exposure, Phys. Rev. Lett. **118**, 021303 (2017).
[5] X. Cui *et al.*, Dark Matter Results From 54-Ton-Day Exposure of PandaX-II Experiment, Phys. Rev. Lett. **119**, 181302 (2017).
[6] R. Ajaj *et al.*, Search for dark matter with a 231-day exposure of liquid argon using DEAP-3600 at SNOLAB, Phys. Rev. D **100**, 022004 (2019).
[7] J. Engel and P. Vogel, Neutralino inelastic scattering with subsequent detection of nuclear gamma-rays, Phys. Rev. D **61**, 063503 (2000).
[8] F. T. Avignone, R. L. Brodzinski, H. S. Miley, J. H. Reeves, A. A. Klimenko, S. B. Osetrov, A. A. Smolnikov, and S. I. Vasilev, Results of the pilot experiment to search for inelastic interactions of WIMPs with Ge-73, Yad. Fiz. **63**, 1337 (2000) [Phys. At. Nucl. **63**, 1264 (2000)].
[9] L. Baudis, G. Kessler, P. Klos, R. F. Lang, J. Menéndez, S. Reichard, and A. Schwenk, Signatures of dark matter scattering inelastically off nuclei, Phys. Rev. D **88**, 115014 (2013).
[10] M. Pospelov, S. Rajendran, and H. Ramani, Metastable nuclear isomers as dark matter accelerators, Phys. Rev. D **101**, 055001 (2020).
[11] B. Lehnert, M. Hult, G. Lutter, and K. Zuber, Search for the decay of nature's rarest isotope $^{180\,m}$Ta, Phys. Rev. C **95**, 044306 (2017).
[12] H. Ejiri and T. Shima, K-hindered beta and gamma transition rates in deformed nuclei and the half-life of $^{180\,m}$Ta, J. Phys. G **44**, 065101 (2017).
[13] H. Ejiri, J. Suhonen, and K. Zuber, Neutrino-nuclear responses for astro-neutrinos, single beta decays and double beta decays, Phys. Rep. **797**, 1 (2019).
[14] Brookhaven National Laboratory National Nuclear Data Center, Nudat (nuclear structure and decay data), 2008.
[15] D. McCammon, R. Almy, E. Apodaca, W. B. Tiest, W. Cui, S. Deiker, M. Galeazzi, M. Juda, A. Lesser, T. Mihara *et al.*, A high spectral resolution observation of the soft x-ray diffuse background with thermal detectors, Astrophys. J. **576**, 188 (2002).
[16] J. Rich, R. Rocchia, and M. Spiro, A search for strongly interacting dark matter, Phys. Lett. B **194**, 173 (1987).
[17] A. L. Erickcek, P. J. Steinhardt, D. McCammon, and P. C. McGuire, Constraints on the interactions between dark matter and baryons from the x-ray quantum calorimetry experiment, Phys. Rev. D **76**, 042007 (2007).
[18] D. Hooper and S. D. McDermott, Robust constraints and novel gamma-ray signatures of dark matter that interacts strongly with nucleons, Phys. Rev. D **97**, 115006 (2018).
[19] V. De Luca, A. Mitridate, M. Redi, J. Smirnov, and A. Strumia, Colored dark matter, Phys. Rev. D **97**, 115024 (2018).
[20] J. Bramante, P. J. Fox, G. D. Kribs, and A. Martin, Inelastic frontier: Discovering dark matter at high recoil energy, Phys. Rev. D **94**, 115026 (2016).
[21] M. Hult, J. Gasparro, G. Marissens, P. Lindahl, U. Wätjen, P. N. Johnston, C. Wagemans, and M. Köhler, Underground search for the decay of ^{180}Ta^{m}, Phys. Rev. C **74**, 054311 (2006).
[22] M. Hult, J. S. E. Wieslander, G. Marissens, J. Gasparro, U. Wätjen, and M. Misiaszek, Search for the radioactivity of 180 mTa using an underground HPGe sandwich spectrometer, Appl. Radiat. Isot. **67**, 918 (2009).
[23] G. Lutter, M. Hult, G. Marissens, H. Stroh, and F. Tzika, A gamma-ray spectrometry analysis software, Appl. Radiat. Isot. **134**, 200 (2018).
[24] A. Caldwell, D. Kollár, and K. Kröninger, Bat—The Bayesian analysis toolkit, Comput. Phys. Commun. **180**, 2197 (2009).
[25] D. A. Neufeld, G. R. Farrar, and C. F. McKee, Dark Matter that interacts with baryons: Density distribution within the Earth and new constraints on the interaction cross-section, Astrophys. J. **866**, 111 (2018).
[26] See Supplemental Material at http://link.aps.org/supplemental/10.1103/PhysRevLett.124.181802 for which includes Refs. [27–29].
[27] J. B. Cumming and D. E. Alburger, Search for the decay of ^{180}Ta^{m}, Phys. Rev. C **31**, 1494 (1985).
[28] G. W. Kim, S. Y. Park, I. S. Hahn, Y. D. Kim, M. H. Lee, D. S. Leonard, E. K. Lee, W. G. Kang, E. Sala, and V. Kazalov,

Simulation study for the half-life measurement of $^{180\,m}$Ta using HPGe detectors, J. Korean Phys. Soc. **75**, 32 (2019).

[29] M. Boswell, Y.-D. Chan, J. A Detwiler, P. Finnerty, R. Henning, V. M. Gehman, R. A. Johnson, D. V. Jordan, K. Kazkaz, M. Knapp *et al.*, MaGe-a GEANT4-based Monte Carlo application framework for low-background germanium experiments, IEEE Trans. Nucl. Sci. **58**, 1212 (2011).

[30] G. Angloher, A. Bento, C. Bucci, L. Canonica, X. Defay, A. Erb, F. von Feilitzsch, N. Ferreiro Iachellini, P. Gorla, A. Gütlein *et al.*, Results on light dark matter particles with a low-threshold cresst-ii detector, Eur. Phys. J. C **76**, 25 (2016).

[31] C. Amole, M. Ardid, D. M. Asner, D. Baxter, E. Behnke, P. Bhattacharjee, H. Borsodi, M. Bou-Cabo, S. J. Brice, D. Broemmelsiek *et al.*, Dark matter search results from the PICO-60CF_3 I bubble chamber, Phys. Rev. D **93**, 052014 (2016).

[32] M. Amman, Optimization of amorphous germanium electrical contacts and surface coatings on high purity germanium radiation detectors, 2018.

[33] D. Protic, E. L. Hull, T. Krings, and K. Vetter, Large-volume Si(Li) orthogonal-strip detectors for Compton-effect-based instruments, IEEE Trans. Nucl. Sci. **52**, 3181 (2005).

[34] T. Irimatsugawa, S. Hatakeyama, M. Ohno, H. Takahashi, C. Otani, and T. Maekawa, High energy gamma-ray spectroscopy using transition-edge sensor with a superconducting bulk tantalum absorber, IEEE Trans. Appl. Supercond. **25**, 1 (2015).

[35] S. A. Karamian, C. B. Collins, J. J. Carroll, and J. Adam, Isomeric to ground state ratio in the ^{180}Ta^{m} (γ, γ) ^{180}Ta^{m,g} reaction, Phys. Rev. C **57**, 1812 (1998).

[36] S. A. Karamian, C. B. Collins, J. J. Carroll, J. Adam, A. G. Belov, and V. I. Stegailov, Fast neutron induced depopulation of the ^{180}Ta^{m} isomer, Phys. Rev. C **59**, 755 (1999).

[37] R. K. J. Sandor, H. P. Blok, M. Girod, M. N. Harakeh, C. W. de Jager, V. Yu Ponomarev, and H. de Vries, Shape transition of 146nd deduced from an inelastic electron-scattering experiment, Nucl. Phys. **A551**, 378 (1993).